Applied Catalysis B: Environmental 99 (2010) 321–328

Contents lists available at ScienceDirect

Applied Catalysis B: Environmental

journal homepage: www.elsevier.com/locate/apcatb

Mechanistic and kinetic insights into the wet air oxidation of phenol with oxygen (CWAO) by homogeneous and heterogeneous transition-metal catalysts

Francesco Arena*, Cristina Italiano, Antonino Raneri, Concetta Saja

Dipartimento di Chimica Industriale e Ingegneria dei Materiali, Università degli Studi di Messina, Viale F. Stagno D'Alcontres 31 c.p. 29, I-98166 Messina, Italy

ARTICLE INFO

Article history:
Received 19 May 2010
Received in revised form 18 June 2010
Accepted 23 June 2010
Available online 30 June 2010

Keywords:
Catalytic wet air oxidation (CWAO)
Phenol
Homogeneous and heterogeneous catalysis
Transition-metals
Reaction mechanism and kinetics
Metal-leaching

ABSTRACT

The activity–selectivity pattern of homogeneous (Cu^{2+}, Fe^{3+}, Mn^{2+}) and ceria-supported ($CuCeO_x$, $MnCeO_x$) transition-metal catalysts in the wet air oxidation of phenol (CWAO) has been probed using a stirred batch reactor with continuous oxygen feeding (T, 150 °C; P_{O_2}, 0.9 Mpa). Both non-catalytic and catalytic homogeneous wet air oxidations proceed *via* an unselective autocatalytic free-radical path leading mostly to refractory C1–C2 acids, while a Langmuir–Hinshelwood (L–H) mechanism accounts for the superior CWAO performance of the $MnCeO_x$ system. A thorough kinetic analysis of the studied systems on the basis of homogeneous autocatalytic free-radical and heterogeneous surface L–H reaction paths has been addressed. The kinetic constants of the various reaction steps show that the $MnCeO_x$ system prompts a fast adsorption of phenol with the consequent abatement of TOC, though a slow oxidation rate determines the buildup of carbonaceous deposits on the catalyst surface. Lower oxidation strength and extensive leaching definitively argue against Cu-based catalysts for the CWAO process.

1. Introduction

The huge variety of organic chemicals made available by the modern chemical industry decisively contributed to the incessant technological progress of the last decades. However, strong toxicity and low biodegradability imply that improper disposal and/or release of many of such substances often constitute a serious threat for environment and human health [1–4]. On this account, novel technologies for decontamination of industrial wastewaters and polluted water resources are currently under scrutiny [1–7].

Among currently available alternatives, wet oxidation processes ensure the highest performances allowing the abatement of many refractory and noxious organic pollutants [1–7]. Nevertheless, the use of costly oxidants (H_2O_2, $KMnO_4$, O_3, UV/γ-irradiation, etc.) limits the feasibility of advanced oxidation processes (AOP) to small-scale applications (e.g., low COD loads and small flow rates), while the wet air oxidation (WAO) requires very demanding conditions to get adequate efficiencies [1–3,5–7]. Although solid catalysts allow overcoming the main drawbacks of the WAO [1–7], the discovery of low-costly active, selective and stable catalysts still remains the main drawback for an extensive application of catalytic wet air oxidation (CWAO) processes [3,4,7]. That is because current catalyst formulations mostly includes costly noble-metals [1–3,5–7], while fouling [3,4,8–12,17] and/or leaching [13–17] phenomena hinder the activity of transition-metal systems. Beside to deactivation and secondary pollution problems, metal-leaching also enables a homogeneous reaction path "masking" the intrinsic CWAO pattern of solid catalysts [13–18]. Then, the lack of comparative studies on mechanisms and kinetics of both homogeneous and heterogeneous transition-metal catalysts, the routine detection of C1–C2 acidic intermediates and peculiar reaction kinetics, often characterized by an initial induction time, are usually taken as proofs of the same autocatalytic free-radical path driven by either homogeneous or heterogeneous transition-metal catalysts [4–7,13–21]. However, the common view on the working mechanism of solid catalysts that, enhancing the rate of O-radicals formation, mostly drive a surface-assisted homogeneous reaction path [5–8,13,17,20–24], contrasts some recent findings on the reactivity pattern of $MnCeO_x$ catalysts arguing a crucial role of surface adsorption in the CWAO of phenol [9–12]. Such a controversial role of solid catalysts coupled to the lack of definitive scientific clues into reaction mechanism and kinetics hinder significant advances towards design and development of robust and effective CWAO catalysts [1,4–7].

Therefore, this study is aimed at providing a comprehensive overview of the catalytic pattern of homogeneous (Fe^{3+}, Cu^{2+}, Mn^{2+}) and ceria-supported ($CuCeO_x$, $MnCeO_x$) transition-metals in the wet air oxidation (CWAO) of phenol, shedding lights into the

* Corresponding author. Tel.: +39 090 676 54 84; fax: +39 090 391 518.
E-mail address: Francesco.Arena@unime.it (F. Arena).

0926-3373/$ – see front matter © 2010 Elsevier B.V. All rights reserved.
doi:10.1016/j.apcatb.2010.06.039

Table 1
Physico-chemical properties of the heterogeneous $MnCeO_x$ and $CuCeO_x$ catalysts.

Catalyst	Metal loading		SA_{BET} (m^2/g)	PV (cm^3/g)	APD (nm)
	Me_{at}/Ce_{at}	(wt.%)			
$CuCeO_x$	0.10	4.1	128	0.26	21
$MnCeO_x$	1.00	21.2	101	0.24	10

relative reaction mechanism. A systematic kinetic analysis of the CWAO pattern shows that the superior efficiency of the $MnCeO_x$ system relies on the occurrence of a typical heterogeneous L–H reaction path, while extensive metal-leaching and low mineralization efficiency definitively prove the unsuitability of Cu-based catalysts for CWAO processes.

2. Experimental

2.1. Materials

$Fe(SO_4)_3$ (>99%, Fluka Chemika), $MnSO_4{\cdot}H_2O$ (>99.5%, Fluka Chemika) and $CuSO_4$ (>98%, Carlo Erba) were used as homogeneous catalysts, while $MnCeO_x$ (Mn_{at}/Ce_{at}, 1) [11,12] and $CuCeO_x$ (Cu_{at}/Ce_{at}, 0.1) [13–15] catalysts were prepared *via* the co-precipitation route, according to the procedures elsewhere described. The physico-chemical properties of the solid catalysts are summarized in Table 1.

2.2. Methods

Catalytic tests in the wet air oxidation of phenol were carried out at 150 °C and a total pressure of 1.4 MPa (P_{O_2}, 0.9 MPa) using a PTF-lined autoclave (0.25 L) equipped with a magnetically driven turbine impeller (≈1000 rpm). The reactor was loaded with a 0.15 L of distilled water containing 1000 ± 50 ppm (≈0.15 g) of phenol and fed with a continuous oxygen flow at the rate of 0.1 stp L min^{-1}. The concentration of homogeneous catalysts was varied in the range of 1–10 ppm, while the load of heterogeneous systems was fixed at 5000 ppm (0.75 g) [11,12]. Liquid samples were withdrawn from the reactor and analysed in terms of: (i) pH; (ii) [Mn^{2+}], [Fe^{3+}] or [Cu^{2+}] by atomic absorption spectrometry (AAS); (iii) phenol and intermediates by HPLC (Mod. *UVD17OU*, *DIONEX*) equipped with a C6-Phenyl 110A column and a dual-channel UV–vis detector and (iv) TOC by a combustion–nondispersive IR analyzer (Mod. *TOC-VCSN*, *SHIMADZU*).

Volatile organic compounds stripped away from the reactor were trapped by bubbling the outlet gaseous flow in a cold (4 °C) water trap (≈10 mL), which was periodically analysed by HPLC and TOC measurements. In addition, the CO_2 selectivity was probed by gravimetric analyses of the precipitated $BaCO_3$ formed by further bubbling the outlet gaseous stream coming from the cold-trap into a saturated $Ba(OH)_2$ solution [11,12]. Selectivity data were calculated by the following formula:

$$S_{CO_2} = \frac{\frac{W_{BaCO_3}\cdot n_C\cdot 12}{MW_{BaCO_3}}}{\frac{W_{PhOH,in}\cdot n_C\cdot 12}{MW_{PhOH}}} \quad (1)$$

where W_{BaCO_3}–$W_{PhOH,in}$ are the weight of the precipitated $BaCO_3$ and the initial weight of phenol, n_C is the number of contained carbon atoms and MW_{BaCO_3}–$MW_{PhOH,in}$ are the molecular weight of $BaCO_3$ and phenol, respectively.

Thermogravimetric (TGA-DSC) analyses of the "used" $CuCeO_x$ and $MnCeO_x$ catalysts were performed using a Simultaneous Thermal Analysis Instrument (Mod. *STA 409C*, *NETZSCH*) operating in air with a heating rate of 5 °C/min.

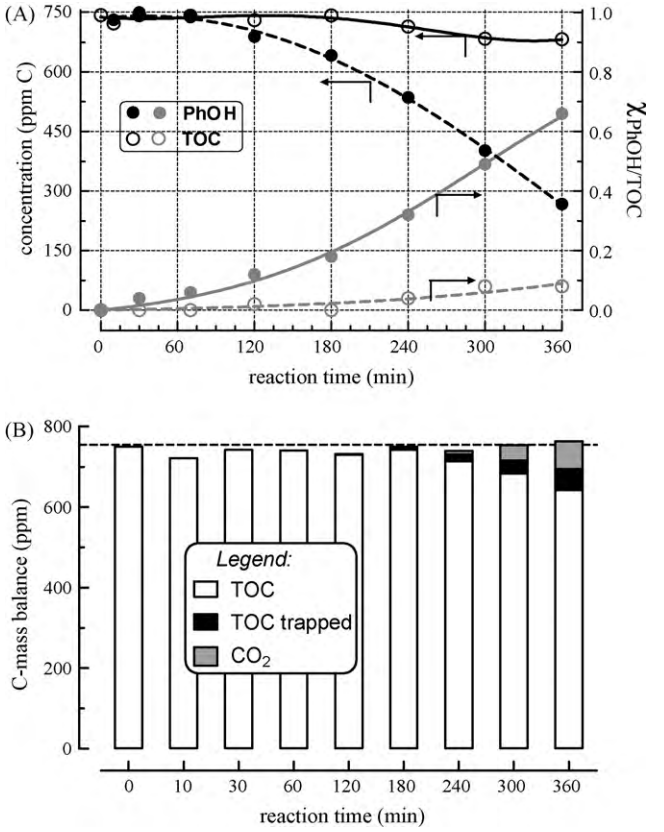

Fig. 1. Blank test data in the wet air oxidation of phenol at 150 °C. (A) concentration and conversion of phenol and TOC *vs.* reaction time; (B) C-mass balance *vs.* reaction time.

3. Results and discussion

3.1. Homogeneous non-catalytic wet air oxidation

The time trends of phenol and TOC concentration and conversion (Fig. 1A) and the carbon-mass balance (Fig. 1B) in the non-catalytic wet oxidation of phenol at 150 °C and 1.4 MPa pressure (i.e., blank test), during 6 h of reaction time, are shown in Fig. 1. The phenol conversion in absence of catalyst depicts a "hollow" trend with a very low rate until the third hour ($\chi_{PhOH} \approx 10\%$), rising more sharply thereafter until a final χ_{PhOH} value of ca. 65% (after 6 h). In the same time, the TOC conversion rises much more slowly with a featureless trend, getting a final value of ca. 10%. Carbon-mass balance data (Fig. 1B) confirm that the removal of TOC parallels the formation of CO_2 (9%) while the TOC analyses of the cold-trap solution signals an incipient stripping of C-containing species (<5%) by the oxygen flow. Such figures account for an accurate C-mass-balance (100 ± 5%) that keeps at comparable levels throughout all the homogeneous tests.

The substrate and product concentration as a function of reaction time (Fig. 2A) along with the 1st-derivative curves of product concentration, corresponding to the relative rate of formation/consumption (Fig. 2B), are shown in Fig. 2. Beside to a low phenol conversion rate, the formation of many intermediates substantiates a poor efficiency of the WAO process in the mineralization of phenol [1,3,5,6,14,15,22]. Indeed, the formation of oxidized C6-aromatic (e.g., cathecol, hydroquinone and benzoquinone) at the earliest stages of the process denotes the primary insertion of a hydroxyl group in the orto (cathecol) and para (hydroquinone) positions of the aromatic ring of the substrate [5,16,18,23]. These undergo a further oxidation to benzoquinones but their concentration keeps very low (Fig. 2) because their

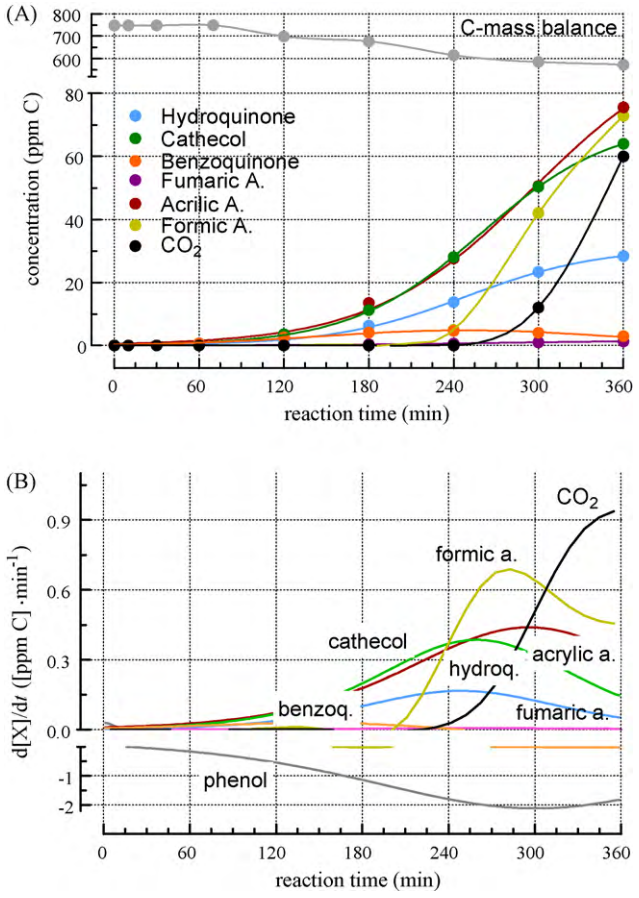

Fig. 2. Blank test data in the wet air oxidation of phenol at 150 °C. (A) concentration of the various intermediates *vs.* reaction time; (B) rate of formation of the various intermediates *vs.* reaction time.

enhanced reactivity [5,6,16,18,23,24] prompts the easy rupture of the aromatic ring leading to the formation of acrylic acid (Fig. 2). A positive rate of formation during all the reaction time accounts for the poor reactivity of the latter compound under WAO conditions. Then, the formation of lower molecular weight intermediates occurs *via* a parallel reaction path still involving the above aromatic intermediates in the presence of a higher concentration of O-radical species, as shown by the following simplified mass balance:

$$(\text{phenol})\, C_6H_5OH + O^{\bullet} \rightarrow C_6H_6O_2\,(\text{dihydroxyl-benzenes}) \quad (a)$$

$$C_6H_6O_2 + O^{\bullet} \rightarrow C_6H_4O_2\,(\text{benzoquinones}) + H_2O \quad (b)$$

$$C_6H_4O_2 + 2HO^{\bullet} \rightarrow 2\,C_3H_3O_2^{-}\,(\text{acrylic acid}) \quad (c)$$

$$C_6H_4O_2 + 2HO^{\bullet} + 2O^{\bullet} \rightarrow C_4H_3O_4^{-} + C_2H_3O_2^{-}\,(\text{maleic} + \text{acetic acids}) \quad (d)$$

$$C_6H_4O_2 + 6O^{\bullet} \rightarrow C_4H_3O_4^{-} + C_2O_4H^{-}\,(\text{maleic} + \text{acetic acid}) \quad (e)$$

$$C_6H_4O_2 + 2HO^{\bullet} + 8O^{\bullet} \rightarrow 6HCOO^{-}\,(\text{formic acid}) \quad (f)$$

$$C_6H_4O_2 + 12O^{\bullet} \rightarrow 6CO_2 + 2H_2O \quad (g)$$

In fact, the matching of the 1st-derivative curve of benzoquinones with the onset formation of formic acid and CO_2 (Fig. 2B) signals that these intermediates play an active role in the main reaction pathway, likely favouring the O-radical chain propagation [3,5,6,22,23,25]. A positive rate of formation during all the reaction time (Fig. 2B) substantiates the scarce reactivity of low-molecular weight C1–C3 acids which hinders the further mineralization of TOC (Fig. 1A), reflecting in an incipient maximum in the rate of CO_2 formation (Fig. 2B). Further, the fact that after ca. 3 h the overall rate of product formation is lower than that of phenol consumption denotes a deficit in C-mass balance up to a final value of ca. 150 ppm (Fig. 2A). Taking into account a concomitant dark-brownish colour of the solution, this finding is diagnostic of the ongoing formation of heavy condensation products from the aromatic intermediates undetected by HPLC analyses [18].

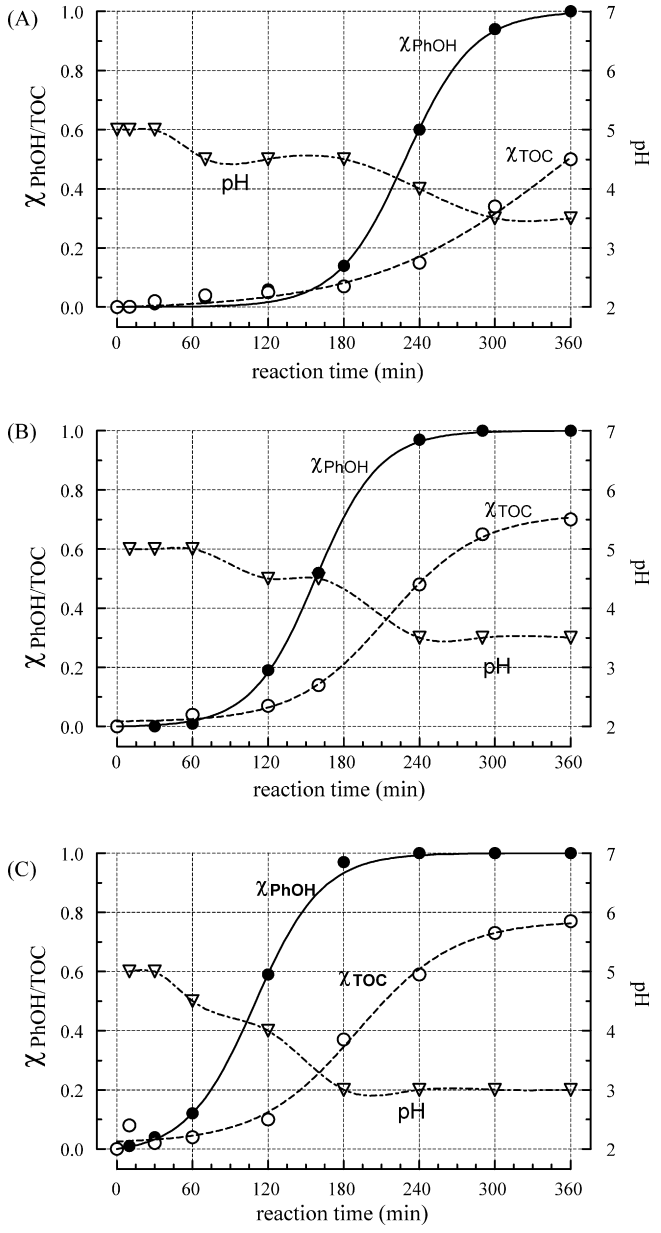

Fig. 3. Homogeneous CWAO of phenol at 150 °C with Fe^{3+} at a concentration of 1 ppm (A), 5 ppm (B) and 10 ppm (C). Phenol and TOC conversion and pH *vs.* reaction time.

3.2. *Wet air oxidation by homogeneous Fe^{3+}, Cu^{2+} and Mn^{2+} catalysts*

The trends of phenol and TOC conversion, of pH and [Fe^{3+}] using the Fe^{3+} catalyst in the concentration range of 1–10 ppm are shown in Fig. 3. In addition, the product distribution at 20%, 50% and 100% phenol conversion is given in Table 2.

A complete conversion of the substrate along with an extent of TOC removal of 50–75% indicate that Fe^{3+} ions promote the wet

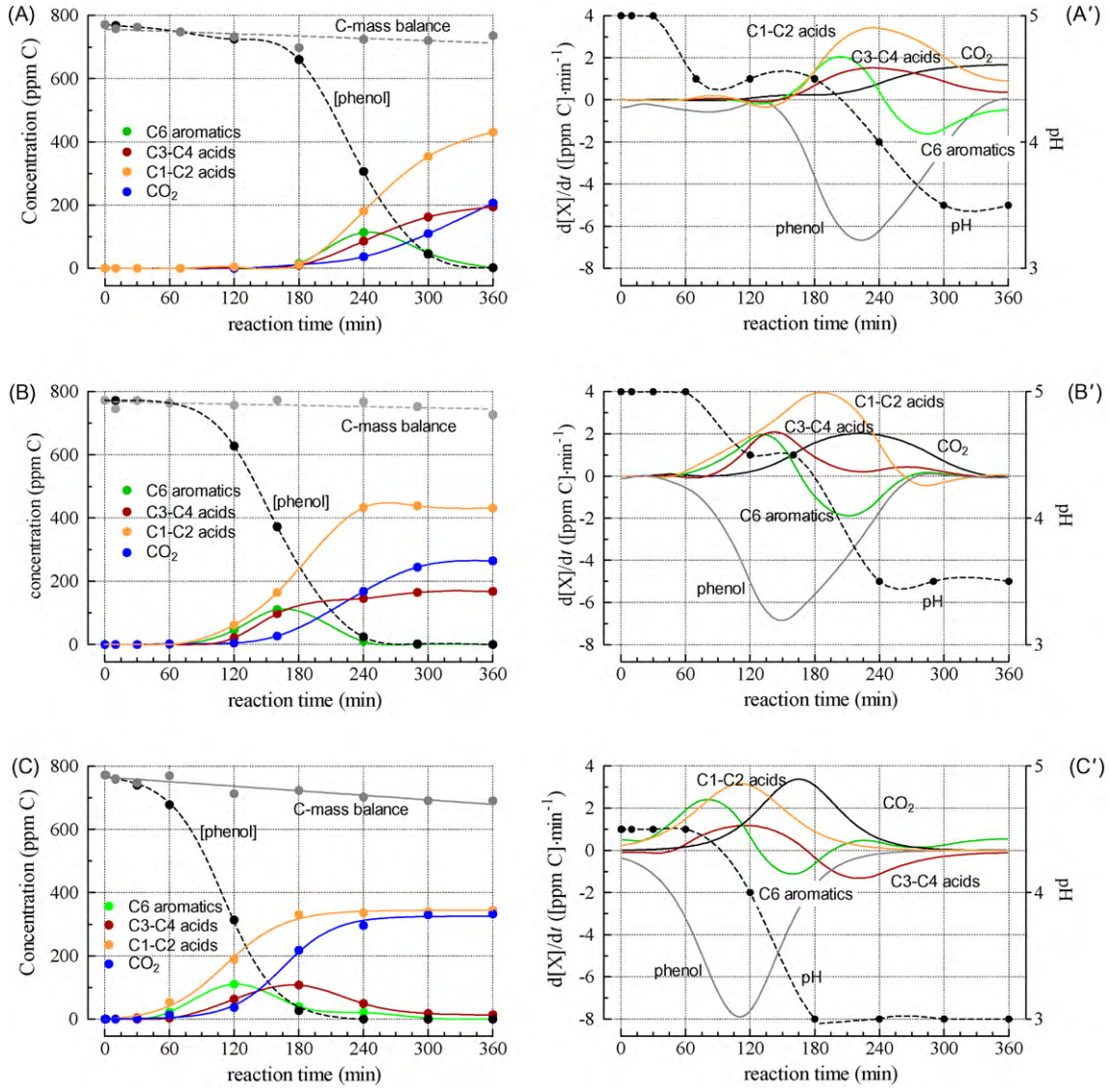

Fig. 4. Homogeneous CWAO of phenol at 150 °C with Fe^{3+} at a concentration of 1 ppm (A, A′), 5 ppm (B, B′) and 10 ppm (C, C′). Concentration of the various intermediates *vs.* reaction time (A–C) and rate of formation of the various intermediates *vs.* reaction time (A′–C′).

Table 2
Selectivity at different phenol conversion levels in homogeneous CWAO tests.

Catalyst (ppm)	X_{PhOH}	Product selectivity (%)										
		Hyq.	Cath.	Bzq.	Mln. a.	Fum. a.	Mal. a.	Acr. a.	Oss. a.	Ac. a.	For. a.	CO_2
Fe^{3+}(1)	0.2	8	12	21	0	0	0	26	0	0	33	0
	0.5	8	15	4	2	0	0	18	0	14	29	9
	1.0	0	0	0	9	0	0	4	1	41	16	28
Fe^{3+}(5)	0.2	7	15	14	0	0	0	16	0	0	47	0
	0.5	8	15	4	7	0	0	18	0	10	31	7
	1.0	0	0	0	9	0	0	1	1	48	6	35
Fe^{3+}(10)	0.2	7	10	17	0	0	4	0	0	0	62	0
	0.5	6	11	3	7	0	4	0	0	19	27	23
	1.0	0	0	1	2	0	0	0	0	25	27	45
Mn^{2+}(5)	0.2	10	5	23	0	1	0	61	0	0	0	0
	0.5	12	26	8	0	1	0	37	0	0	0	16
	1.0	0	1	0	0	0	0	12	2	47	11	27
Cu^{2+}(5)	0.5	7	11	7	0	0	0	21	1	46	7	0
	1.0	0	0	0	0	0	0	0	1	48	2	49

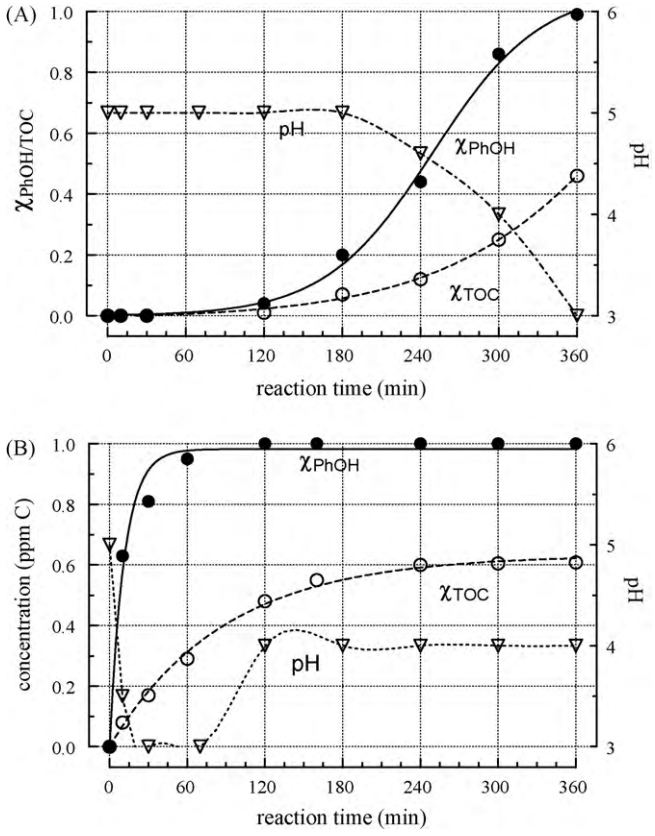

Fig. 5. Homogeneous CWAO of phenol at 150 °C with Mn^{2+} (A) and Cu^{2+} (B) catalysts (5 ppm). Phenol and TOC conversion and pH *vs.* reaction time.

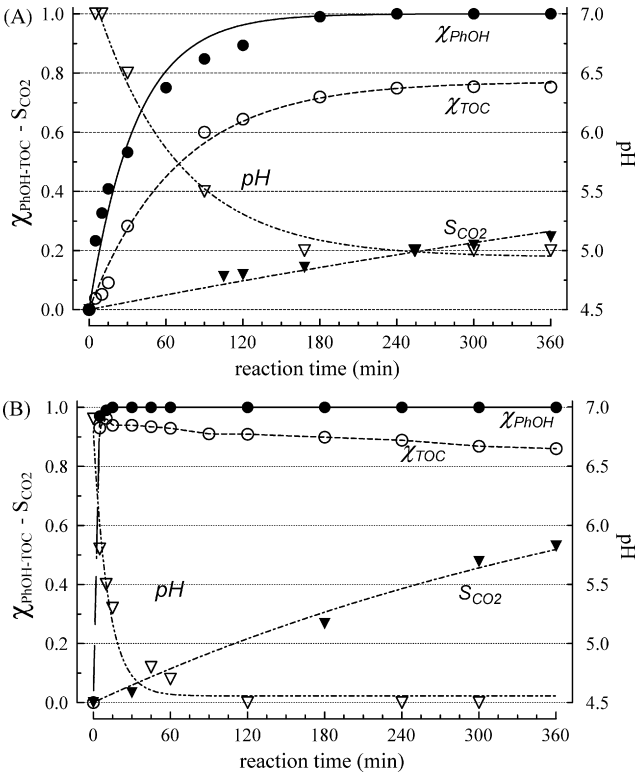

Fig. 6. Heterogeneous CWAO of phenol at 150 °C on $CuCeO_x$ (A) and $MnCeO_x$ (B) catalysts. Phenol and TOC conversion, pH and CO_2 selectivity *vs.* reaction time.

air oxidation of phenol even at a concentration of 1 ppm (Fig. 3A), according to the recognised effect of Fe ions leached from the reactor (ca. 1 ppm) in the wet air oxidation of hydroquinone [18]. Although an induction time longer than that recorded in the blank test (Fig. 1) signals a peculiar inhibiting effect at lower (<10 ppm) concentration, it is evident a progressive reduction of both the induction time (2 h → 0) and time required (6 → 4 h) to get a full phenol conversion with rising the concentration (Fig. 3). The product distribution and the relative rate of formation/consumption *vs.* reaction time, shown in Fig. 4, indicate that a higher phenol conversion rate reflects in an increased selectivity to CO_2 and C1–C2 acids at expense of C3–C4 ones (see Fig. 4 and Table 2), substatiating a stronger oxidative pattern at higher Fe^{3+} concentrations.

Irrespective of concentration, during ca. 1 h from the onset of phenol conversion the reaction rate increases steadily up to a conversion level of ca. 50% (Fig. 4) reflecting in a simultaneous increase in the concentration of all the intermediates, still according to a consecutive-parallel reaction path *via* the primary formation of hydro- and benzoquinones [1,3,5,6,14–18]. At this time the rate of C6 formation attains the maximum, becoming quickly negative (i.e., consumption) owing to an increasing consumption rate during the fastest kinetic regime, likely enabled by a higher concentration of organic compounds able to promote the radical chain propagation [15,22,23]. At the highest Fe^{3+} concentration (Fig. 4C and C′) also the rate of formation of the C3–C4 intermediates becomes negative (consumption), according to the prevailing production of CO_2 and, mostly of C1–C2 acids (Table 2) accounting for the asymptotic value in TOC conversion and lower final pH values (Fig. 3B and C). Overall, such findings signal a direct activity–selectivity relationship in the homogeneous wet air oxidation of phenol that is confirmed by conversion and kinetic data of the homogeneous Mn^{2+} and Cu^{2+} catalysts, at the fixed concentration of 5 ppm, shown in Fig. 5. The former species (Fig. 5A) presents an activity pattern similar to Fe^{3+}, also in terms of a comparable (≈2 h) induction time, while a higher production of acrylic acid, coupled to a lower production of formic acid and CO_2, substantiates the poor oxidation strength of the Mn^{2+} species (Table 2). According to the literature data [3,4,14–16], a very short, if any, induction time and the attainment of a complete phenol conversion in ca. 2 h prove the highest CWAO activity of the Cu^{2+} species (Fig. 5B). Although a higher selectivity to CO_2 (Table 2) substantiates the strongest oxidation pattern of Cu^{2+} [1,3,5–7], the overwhelming production of acetic acid denotes a poor efficiency of the homogeneous CWAO towards such refractory intermediate [1–6,16,18,23].

3.3. *Wet air oxidation by heterogeneous $CuCeO_x$ and $MnCeO_x$ catalysts*

The $CuCeO_x$ (Fig. 6A) and, mostly, $MnCeO_x$ (Fig. 6B) systems show a quite different behavior pattern in terms of both phenol and TOC removal and product selectivity (Table 3).

The former leads to the complete disappearance of phenol after ca. 3 h, while the TOC conversion rises with a similar trend to an asymptotic value of ca. 75%, keeping unchanged during the subsequent 3 h. The pH decreases from 7 to ca. 5 with an opposite trend, while a steady rate of formation (0.39 $mmol_{CO_2}\ h^{-1}$) results in a final CO_2 selectivity value of only ca. 25% that points to a ca. 50% deficit in the C-mass balance. The product distribution indicates that the residual TOC is related to the accumulation of refractory C1–C2 acids (Table 3), in agreement with the observed pH decrease (Fig. 6A).

The $MnCeO_x$ catalyst features a superior CWAO performance with a simultaneous removal of substrate and TOC in ca. 20 min (Fig. 6B). Thereafter phenol is not longer detected though a slight and progressive increase of TOC (χ_{TOC}, 97 → 85%) is evident. The pH decreases to a value of ca. 4.5 during the first 2 h, keeping

Table 3
Selectivity in heterogeneous CWAO tests based on TOC and CO_2 at various times.

Catalyst	Time (h)	Product selectivity (%)										
		Hyq.	Cat.	Bzq.	Mln. ac.	Fum. ac.	Mal. ac.	Acr. ac.	Oss. ac.	Ac. ac.	For. ac.	CO_2
$CuCeO_x$	1	1	9	11	27	0	0	0	12	19	0	21
	3	1	0	0	12	0	0	0	11	41	0	35
	6	0	0	0	0	0	0	0	7	47	0	46
$MnCeO_x$	1	1	0	0	0	0	0	0	0	5	28	67
	3	3	0	0	0	0	0	0	0	7	24	69
	6	0	0	0	0	0	0	0	0	9	20	71

unchanged until the end of the run, in agreement with the formation of acetic and formic acids (Table 3). Furthermore, a constant rate of CO_2 formation (0.91 $mmol_{CO_2}$ h^{-1}), more than two times higher than that of previous system, results in a final CO_2 selectivity of ca. 55% (Fig. 6B) pointing out also in this case a considerable gap between TOC conversion (ca. 85%) and CO_2 production that corresponds to a ca. 30% deficit in C-mass balance.

This prompted us to probe the presence of C-containing species on the "used" catalysts by TGA-DSC measurements [4,8–12,21]. The results (see Supplementary information) outline a weight loss of ca. 7 and 10% for $MnCeO_x$ and $CuCeO_x$ catalysts respectively, in concomitance with an exothermic DSC signal [11,12] indicating that a considerable fraction of TOC is strongly adsorbed at the catalyst surface being oxidized to CO_2 at $T > 150\,^{\circ}C$ [9–12]. Although under comparable reaction conditions Hočevar et al. recorded the presence of a much lower amount of adsorbed carbon (0.2–3.9 wt%) on the used $CuCeO_x$ catalysts, in our case a much higher surface area explains the major fraction of adsorbed carbonaceous deposits [13]. Anyway, TGA data allow for a reliable C-mass balance ($100 \pm 5\%$) also for the heterogeneous systems.

At least, despite of the similar final pH of the reacting solution (Fig. 6), also the resistance to leaching of the two systems is markedly different. Indeed, for the $MnCeO_x$ sample the Mn leaching was negligible (ca. 2 ppm corresponding to less 0.2% of the Mn loading) throughout the run, while for the $CuCeO_x$ catalyst the Cu^{2+} attained a concentration level of 50 ppm in the first hour, leveling off thereafter to a steady concentration of ca. 20 ppm, accounting for a major loss (10–25%) of active phase [13–18].

3.4. Mechanistic and kinetic insights into homogeneous and heterogeneous CWAO of phenol

The different CWAO pattern of the homogeneous Fe, Mn and Cu catalysts can be explained considering the main aspects of their aqueous chemistry. In particular, since the radical-chain initiation is prompted by the interaction of molecular oxygen with electron-donor species (i.e., the substrate) [5,6,18,22–24], the efficiency of the various transition-metal ions mirrors their ability to promote the electron-transfer, shifting between two or more allowed oxidation states [1,5,6]. On this account, the long induction time recorded with Fe^{3+} and Mn^{2+} catalysts signals that at lower concentration (<10 ppm) such species somewhat act as inhibitor of the radical-chain initiation. At the opposite, a very short induction time points to a very effective working mechanism of the Cu^{2+} species on the radical-chain initiation and propagation. This is probably ascribable to a very favourable redox potential ($E_{Cu^{2+}/Cu^{+}}$, 0.171 eV at 25 °C) promoting the electron-transfers processes. However, the CWAO efficiency of the Cu^{2+} species probably depends also on its ability to form metal-complexes with several intermediates produced during the wet oxidation of phenol [16–18,26] that further enhances the rate of electron-transfer(s) between oxygen and intermediates [16,18,22]. In this context, the Mn^{2+} and Fe^{3+} species feature a lower ability to drive the radical-chain initiation probably because of less favourable redox potentials ($E_{Fe^{3+}/Fe^{2+}}$, 0.771 eV at pH = 1; $E_{MnO_2/Mn^{2+}}$, 1.229 eV at pH = 1) and their strong tendency to form insoluble precipitates under oxidizing conditions (i.e., Fe_2O_3 and MnO_2), which could act as inhibitor of the radical-chain initiation/propagation in the initial stages of the reaction.

All these findings match the fey-features of the autocatalytic free-radical reaction path, the kinetics of which are described by the following equation [13,20,25]:

$$\chi = \frac{1 - \exp\left[-(A_0 + C_0)\cdot k \cdot t\right]}{1 + \left(\frac{A_0}{C_0}\right)\cdot \exp\left[-(A_0 + C_0)\cdot k \cdot t\right]} \quad (2)$$

where C_0 is the concentration of active radical species, A_0 is the concentration of the substrate (0.0106 mol/L) and k the kinetic constant ($L\,mol^{-1}\,h^{-1}$). Therefore, a comparison of phenol conversion data on the basis of the Eq. (2) would highlight value and meaning of the C_0 and k parameters for both homogeneous and heterogeneous systems. The curve fitting of experimental data by Eq. (2) according to the least-squares fit method is presented in Fig. 7, while values of R^2 and absolute sum of squares of the curve fit and the calculated values of the C_0 and k kinetic parameters are summarized in Table 4. A high accuracy of data fitting (R^2, 0.98–1.00) allows for a reliable comparison of the kinetic parameters of the various systems. The blank test is characterized by the lowest value of the kinetic constant ($81\,L\,mol^{-1}\,h^{-1}$), while regardless of concentration the Fe^{3+} system features a same, three times greater value of k ($205–223\,L\,mol^{-1}\,h^{-1}$), consistent with the same nature of the catalytic active species. The Mn^{2+} ions feature a lower k value ($153\,L\,mol^{-1}\,h^{-1}$) though it is two times larger than that recorded in absence of catalyst while, according to its higher activity, the Cu^{2+} species features the highest kinetic constant ($606\,L\,mol^{-1}\,h^{-1}$) that is more than three times greater than that of Fe^{3+}.

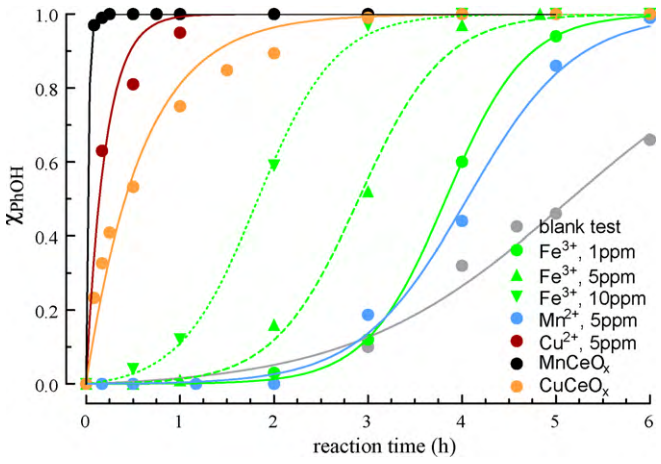

Fig. 7. Fitting of phenol conversion data by the autocatalytic free-radical kinetic model (Eq. (2)).

Table 4
Values of the kinetic parameters provide the significance of the of the autocatalytic free-radical reaction path for homogeneous and heterogeneous wet air oxidation tests (T, 150 °C; A_0, 0.0106 mol L^{-1}).

Catalyst (ppm)		Goodness of fit		C_0	Std error	k	Std error
		R^2	a.s.o.s.[a]	(mol L^{-1})		(L mol^{-1} h^{-1})	
No	–	0.99	2.4E−03	4.6E−05	1.5E−05	81	6
Fe^{3+}	1	1.00	2.7E−03	2.7E−06	1.5E−06	205	13
Fe^{3+}	5	1.00	1.8E−03	2.1E−05	8.2E−06	223	15
Fe^{3+}	10	1.00	1.2E−04	1.8E−04	1.6E−05	208	5
Mn^{2+}	5	1.00	1.3E−03	2.0E−05	5.5E−06	153	7
Cu^{2+}	5	0.98	2.8E−02	1.8E−03	1.1E−01	606	198
$CuCeO_x$	5000	1.00	6.0E−03	4.9E−03	1.7E−03	122	28
$MnCeO_x$	5000	1.00	1.0E−03	2.3E−18	–	2E+16	–

[a] a.s.o.s., absolute sum of squares.

Although a different curve shape, the curve fitting of the $CuCeO_x$ system (Table 4) provides a reasonably low value of the kinetic constant (153 L mol^{-1} h^{-1}), comparing with that of Mn^{2+} according to a similar time (≈4 h) required for the full conversion of phenol (Fig. 7). At variance, an unrealistic value of the kinetic constant equal to ca. 2.0E+16 L mol^{-1} h^{-1} evidently points to the occurrence of a different reaction mechanism driven by the $MnCeO_x$ system [9–15], as further substantiated by a value of the C_0 parameter practically equal to zero (2.3E−18 mol L^{-1}). Accounting for the initial concentration of active radical species [13,25] and the relative length of the induction time (Fig. 7), indeed the C_0 parameter ranges between 2.7E−06 and 4.8E−03 mol L^{-1} for 1 ppm of Fe^{3+} and $CuCeO_x$ system, respectively. In absence of catalyst C_0 is equal to 4.6E−05 mol L^{-1}, resulting even smaller (2.7E−06 to 2.1E−05 mol L^{-1}) for the Mn^{2+} and Fe^{3+} species at concentration lower than 10 ppm, according to the longer induction time recorded in such tests (Fig. 7). Only at higher concentration, in agreement with the disappearance of the induction time, the C_0 value of Fe^{3+} (1.8E−04 mol L^{-1}) becomes substantially greater than that of the blank test, while it is two orders of magnitude greater for Cu^{2+} (1.8E−03 mol L^{-1}) and $CuCeO_x$ (4.8E−03 mol L^{-1}) catalysts. Therefore, the kinetic analysis points to the occurrence of the same homogeneous autocatalytic free-radical reaction path on all the studied systems with the exception of the $MnCeO_x$ catalyst. Indeed, lack of any induction time and sharp rise of phenol and TOC conversion coupled to TGA data of the used samples indicate that the CWAO of phenol on the latter system proceeds *via* a classical heterogeneous Langmuir–Hinshelwood (L–H) mechanism [9–12,27]:

$$\text{Ph–OH} + \alpha \leftrightarrows \text{Ph–OH}_{(s)} \quad \text{(i)}$$

$$\text{Ph–OH}_{(s)} + \sigma\text{–O} \rightarrow P_{(s)} + \sigma \quad \text{(ii)}$$

$$P_{(s)} \leftrightarrows P_{(l)} \quad \text{(iii)}$$

$$P_{(s)} + n\sigma\text{–O} \rightarrow \text{CO}_{x(s)} \quad \text{(iv)}$$

$$P_{(s)} \rightarrow \text{C-deposits} \quad \text{(iv′)}$$

$$\text{CO}_{x(s)} \leftrightarrows \text{CO}_x \quad \text{(v)}$$

$$\sigma + \text{O}_2 \rightarrow \sigma\text{–O} \quad \text{(vi)}$$

The first reaction step consists of the adsorption of the substrate on the catalyst surface (i), well explaining the contemporary removal of phenol and TOC according to a pseudo 1st-order kinetic law [9–12]. The subsequent reaction steps involved by the heterogeneous CWAO process are the surface oxidation of substrate (ii) and intermediates (iv), product desorption (iii) and (v) and catalyst oxygen replenishment (vi) [11,12], while a parasite process leading to buildup of C-deposits (iv′) with consequent catalyst deactivation by fouling has been also considered [9–12,26]. Considering that non-dissociative adsorption far away from equilibrium conditions [25] obeys to a 1st-order kinetic law, phenol and TOC conversion data were fitted by the equation:

$$\chi = 1 - \exp[-k \cdot t] \quad (3)$$

Moreover, also the rate of CO_2 formation was evaluated by such kinetic model and the values of the kinetic constant of phenol (k_{PhOH}) and TOC (k_{TOC}) adsorption and of CO_2 formation (k_{CO_2}) of $CuCeO_x$ and $MnCeO_x$ catalysts are compared in Table 5. The kinetic constants of phenol and TOC adsorption of the $MnCeO_x$ catalyst are equal to 8.4 and 7.7 L g^{-1} h^{-1} respectively, according to the analogous trend with reaction time (Fig. 6B). Values of the kinetic constants lower than those of the previous catalyst by more than one order of magnitude (k_{PhOH}, 0.37 L g^{-1} h^{-1}; k_{TOC}, 0.17 L g^{-1} h^{-1}) and the asymptotic value in TOC conversion (≈75%) are instead consistent with the much poorer CWAO performance of the $CuCeO_x$ system. According to the main features of the above L–H mechanism, it is evident that a k_{TOC}/k_{PhOH} ratio equal to 1 can be taken as a reliable index of the occurrence of the heterogeneous reaction path. Then, a k_{TOC}/k_{PhOH} ratio of 0.92 confirms that the CWAO of phenol on the $MnCeO_x$ catalyst proceeds *via* the L–H path, while the prevalence of the homogeneous reaction path with the $CuCeO_x$ system is confirmed by a k_{TOC}/k_{PhOH} value of 0.46 (Table 5). Indeed, the working mechanism of such a system relies on both the L–H path driven by the surface adsorption of phenol and the homogeneous free-radical path enabled by the extensive Cu^{2+} leaching [14,15].

A final overview of the CWAO efficiency of the various systems is provided by Fig. 8, comparing the final CO_2 selectivity and the residual TOC and the difference between these, corresponding to the fraction of VOC stripped away in homogeneous tests and the amount of adsorbed carbon for the solid catalysts (Supplementary information). These data substantiate that the solid $MnCeO_x$ cata-

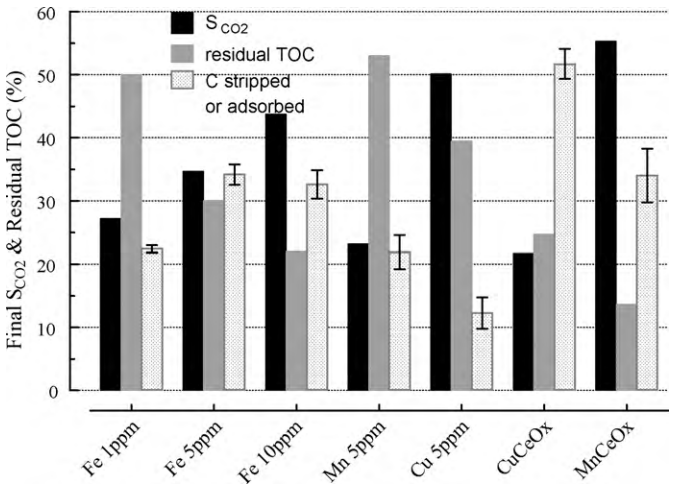

Fig. 8. Overall comparison of the CWAO performance of homogeneous and ceria-supported transition-metal catalysts.

Table 5
Pseudo-first order kinetic constants of phenol and TOC conversion and of CO_2 formation.

Catalyst	$\chi_{PhOH,max}$ (%)	R^2	k_{PhOH} ($L\,g^{-1}\,h^{-1}$)	Std error	$\chi_{TOC,max}$ (%)	R^2	k_{TOC} ($L\,g^{-1}\,h^{-1}$)	Std error	k_{TOC}/k_{PhOH}	R^2	k_{CO_2} ($L\,g^{-1}\,h^{-1}$)	Std error	k_{CO_2}/k_{TOC}
$CuCeO_x$	100	0.97	3.7E−1	0.029	77	0.99	1.7E−1	0.016	0.46	0.96	1.0E−2	4.3E−04	0.059
$MnCeO_x$	100	1.00	8.4E+0	0.228	95	1.00	7.7E+0	1.164	0.92	1.00	2.4E−2	1.2E−03	0.003

lyst is the most effective system, ensuring the fastest and highest removal of substrate and TOC, the highest TOC mineralization and the lowest release of intermediates. However, the strong adsorption of carbonaceous deposits on the catalyst surface leading to a progressive activity decay by fouling represents the main drawback of the $MnCeO_x$ system [3,4,8–12,17], as indicated by very different values of the kinetic constants (Table 5) of surface adsorption (i) and surface oxidation steps (ii and iv). Indeed, the kinetic constant of CO_2 formation for the $MnCeO_x$ and $CuCeO_x$ catalysts are equal to $2.4\,10^{-2}$ and $1.0\,10^{-2}\,L\,g^{-1}\,h^{-1}$ respectively, being smaller than k_{TOC} by 2–3 orders of magnitude (Table 5). In particular, the k_{CO_2}/k_{TOC} ratio is equal to 0.059 for the $CuCeO_x$ characterized by a lower rate of TOC removal due to a slower surface adsorption and the parallel occurrence of the homogeneous reaction path. While despite of the higher rate of CO_2 production, the k_{CO_2}/k_{TOC} ratio for the $MnCeO_x$ system results much lower (0.003) because of the very fast adsorption rate and the lack of any parallel homogeneous reaction network. Anyway, these findings substantiate that the surface oxidation step is the rate limiting step (r.l.s.) of the heterogeneous CWAO of phenol [11,12,27], well accounting for the slight release of low-molecular weight intermediates (Fig. 6B) due to a low CWAO efficiency of the $MnCeO_x$ system towards such refractory intermediates [8–12,21].

Then the main requirements of heterogeneous CWAO catalysts lye in a high water decontamination efficiency due to a fast adsorption capacity that depends on textural and surface chemical properties of the catalyst [9–12], while dispersion and redox properties of the active phase control the oxidation activity of adsorbed C-species determining, at once, mineralization functionality and catalyst stability against fouling [4,8–12,17,21,27]. On the other hand, extensive metal-leaching and low oxidation strength definitively argue against the suitability of Cu-based catalysts for the CWAO process [14–17].

4. Conclusions

The main mechanistic and kinetic aspects of the wet air oxidation of phenol by homogeneous and heterogeneous transition-metal catalysts (CWAO) were addressed in the light of both homogeneous and heterogeneous reaction mechanisms.

Homogeneous catalysts drive an unselective homogeneous free-radical path leading mostly to C1–C2 intermediates, while a typical surface heterogeneous L–H mechanism accounts for the superior CWAO efficiency of the $MnCeO_x$ system.

A fast adsorption of the substrate accounts for the superior water decontamination efficiency of the $MnCeO_x$ system, while a slower oxidation rate of adsorbed species (r.l.s.) determines the selectivity pattern and catalyst stability against fouling phenomena.

The formation of common acidic refractory intermediates, lower intrinsic activity of solid catalysts and metal-leaching phenomena are likely at the origin of the common assumption of a (surface-assisted) homogeneous radical path accounting for the CWAO pattern of heterogeneous transition-metal catalysts.

Appendix A. Supplementary data

Supplementary data associated with this article can be found, in the online version, at doi:10.1016/j.apcatb.2010.06.039.

References

[1] G. Busca, S. Berardinelli, C. Resini, L. Arrighi, J. Hazard. Mater. 160 (2008) 265.
[2] K. Pirkanniemi, K. Sillanpää, Chemosphere 48 (2002) 1047.
[3] S.K. Bhargava, J. Tardio, J. Prasad, K. Foger, D.B. Akolekar, S.C. Grocott, Ind. Eng. Chem. Res. 45 (2006) 1221.
[4] F. Larachi, Top. Catal. 33 (2005) 109.
[5] S. Imamura, Ind. Eng. Chem. Res. 38 (1999) 1743.
[6] Yu.I. Matatov-Meytal, M. Sheintuch, Ind. Eng. Chem. Res. 37 (1998) 309.
[7] F. Luck, Catal. Today 53 (1999) 81.
[8] S.T. Hussain, A. Sayari, F. Larachi, J. Catal. 201 (2001) 153.
[9] M. Abecassis-Wolfovich, M.V. Landau, A. Brenner, M. Herskowitz, Ind. Eng. Chem. Res. 43 (2004) 5089.
[10] M. Abecassis-Wolfovich, R. Jothiramalingam, M.V. Landau, M. Herrskowitz, B. Viswanathan, T.K. Varadarajan, Appl. Catal. B: Environ. 59 (2005) 91.
[11] F. Arena, J. Negro, G. Trunfio, A. Parmaliana, Ind. Eng. Chem. Res. 46 (2007) 6724.
[12] F. Arena, G. Trunfio, J. Negro, L. Spadaro, Appl. Catal. B 85 (2008) 40.
[13] S. Hočevar, J. Batista, J. Levec, J. Catal. 184 (1999) 39.
[14] F. Arena, R. Giovenco, T. Torre, A. Venuto, A. Parmaliana, Appl. Catal. B: Environ. 45 (2003) 51.
[15] F. Arena, E. Alongi, P. Famulari, A. Parmaliana, G. Trunfio, Catal. Lett. 107 (2006) 39.
[16] A. Santos, P. Yustos, A. Quintanilla, F. García-Ochoa, Top. Catal. 33 (2005) 181.
[17] S.-K. Kim, S.-K. Ihm, Top. Catal. 33 (2005) 171.
[18] A. Quintanilla, J. Casas, A.F. Mohedano, J.J. Rodriguez, Appl. Catal. B: Environ. 67 (2006) 206.
[19] Q. Wu, X. Hu, Po-l. Yue, Chem. Eng. Sci. 58 (2003) 923.
[20] J. Pintar, J. Levec, J. Catal. 135 (1992) 345.
[21] H. Chen, A. Sayari, A. Adnot, F. Larachi, Appl. Catal. B 32 (2001) 195.
[22] J. Vicente, R. Rosal, M. Diaz, Ind. Eng. Chem. Res. 41 (2002) 46.
[23] H.R. Devlin, J.J. Harris, Ind. Eng. Chem. Fund 23 (1984) 387.
[24] D. Duprez, F. Delanoë, J. Barbier, P. Isnard, G. Blanchard, Catal. Today 29 (1996) 317.
[25] O. Levenspiel, Chemical Reaction Engineering, 3rd ed., Wiley, NY, 1999.
[26] I.M. Kolthoff, E.B. Sandell, E.J. Mehan, S. Bruckenstein, Quantitative Analytical Chemistry, vol. 1, Piccin Edition, Padua, Italy, 1973.
[27] F. Arena, A. Parmaliana, G. Trunfio, Stud. Surf. Sci. Catal. 72 (2007) 489.